Myosin-dependent endoplasmic reticulum motility and F-actin organization in plant cells

Haruko Ueda[a], Etsuo Yokota[b], Natsumaro Kutsuna[c,d], Tomoo Shimada[a], Kentaro Tamura[a], Teruo Shimmen[b], Seiichiro Hasezawa[c,d], Valerian V. Dolja[e], and Ikuko Hara-Nishimura[a,1]

[a]Department of Botany, Graduate School of Science, Kyoto University, Kyoto 606-8502, Japan; [b]Department of Life Science, Graduate School of Life Science, University of Hyogo, Harima Science Park City, Hyogo 678-1297, Japan; [c]Department of Integrated Biosciences, Graduate School of Frontier Sciences, The University of Tokyo, Kashiwanoha Kashiwa, Chiba 277-8562, Japan; [d]Institute for Bioinformatics Research and Development (BIRD), Japan Science and Technology Agency (JST), Chiyoda-ku, Tokyo 102-0081, Japan; and [e]Department of Botany and Plant Pathology and Center for Genome Research and Biocomputing, Oregon State University, Corvallis, OR 97331

Edited* by Brian A. Larkins, University of Arizona, Tuscon, AZ, and approved February 22, 2010 (received for review October 5, 2009)

Plants exhibit an ultimate case of the intracellular motility involving rapid organelle trafficking and continuous streaming of the endoplasmic reticulum (ER). Although it was long assumed that the ER dynamics is actomyosin-driven, the responsible myosins were not identified, and the ER streaming was not characterized quantitatively. Here we developed software to generate a detailed velocity-distribution map for the GFP-labeled ER. This map revealed that the ER in the most peripheral plane was relatively static, whereas the ER in the inner plane was rapidly streaming with the velocities of up to ~3.5 μm/sec. Similar patterns were observed when the cytosolic GFP was used to evaluate the cytoplasmic streaming. Using gene knockouts, we demonstrate that the ER dynamics is driven primarily by the ER-associated myosin XI-K, a member of a plant-specific myosin class XI. Furthermore, we show that the myosin XI deficiency affects organization of the ER network and orientation of the actin filament bundles. Collectively, our findings suggest a model whereby dynamic three-way interactions between ER, F-actin, and myosins determine the architecture and movement patterns of the ER strands, and cause cytosol hauling traditionally defined as cytoplasmic streaming.

myosin XI | actin filament | cytoplasmic streaming | velocity distribution map | *Arabidopsis thaliana*

Cytoplasmic streaming, defined as an extensive intracellular motility in plants, was first described in 1774 (1). It is thought that unidirectional actin filament (AF) bundles and organelle-associated myosin XI, a plant-specific class of myosin motors, cause bulk flow in the cell (reviewed in refs. 2–4). Some myosin XI were indeed reported to slide along AFs in vitro (5, 6). Using immunocytochemical analyses (7–11) and fluorescent protein-labeled myosins (12, 13), myosin XI have been shown to be associated with the particulate organelles. Recent analyses using gene knockouts and dominant-negative inhibition demonstrated that several class XI myosins have overlapping functions in the rapid movement of organelles (14–18). Among these, myosin XI-K was found to play the most prominent role in the movement of Golgi bodies, peroxisomes, and mitochondria. Studies have also concluded that none of these three organelles fits the paradigm of cytoplasmic streaming, raising the question of what drives this conspicuous process (14, 15).

The endoplasmic reticulum (ER), an organelle present in all eukaryotic cells, harbors the largest reservoir of cellular membranes. Cytoskeleton-dependent remodeling of the ER network, which consists of cisternae and interconnected membrane tubes, is well known in both animals and plants (reviewed in refs. 19–22). In addition, dynamic streaming of the plant ER has been observed in subperipheral cytoplasm and transvacuolar strands (23–25). However, the molecular mechanism underlying the ER streaming is not known, although it was reported that the 175 kDa myosin XI was localized on the ER of tobacco cell culture BY-2 (26).

Unlike the movement of the particulate organelles, quantitative analysis of the ER streaming was long hampered by the inherent difficulty of ER tracking. Here, we measured the ER streaming using recently developed software, and identified an *Arabidopsis* myosin XI-K as the primary contributor to ER streaming. We have also implicated class XI myosins into the organization of the AF bundles and advanced a model according to which rapid, myosin-dependent ER motility along the thick AF bundles is a driver of cytoplasmic streaming.

Results and Discussion

Quantitative Analyses of the ER Movement and Cytoplasmic Streaming. We used the epidermal cells of cotyledonary petioles of the transgenic *Arabidopsis* expressing ER-localized GFP (GFP-h) as a convenient model to follow the ER dynamics. In these cells, we observed a relatively static peripheral ER network and the rapidly moving thick strands with high GFP fluorescent intensities, which we designated as ER strands (Fig. 1*A*, and Movies S1 and S2). The ER strands streamed mostly along the longitudinal axis of the cell (Movies S1 and S2).

To comprehensively analyze the ER movement, we developed a software, KbiFlow plug-in package for ImageJ software, based on the optical-flow analysis. KbiFlow generates a velocity map by calculating the average velocity of 16 × 16 pixels (2.54 × 2.54 μm) in 100 time-lapse images for ~5.4 s (Fig. S1), and makes it possible to estimate not only the velocity and the direction, but also the distribution of the streaming in a wide field. The velocity maps showed that the ER is composed of several regions that move in distinct orientations and with variable velocities within a focal plane (Fig. S2). The velocity maps highlighted the rapidly moving thick ER strands.

For each analyzed cell, we selected two ~1-μm thick optical planes at ~1.5 μm distance, a peripheral plane and an interior plane, and calculated maximum and average ER velocities in each plane. Statistical analysis of 16 cells showed that the maximal ER velocities were 1.35 μm/sec for the cell periphery and 2.20 μm/sec for the cell interior ($P < 0.005$ by Mann-Whitney test), whereas the average velocities were 0.33 μm/sec and 0.48 μm/sec for the cell periphery and interior, respectively ($P < 0.05$ by Mann-Whitney test) (Fig. S2*E* and Table S1). This analysis showed that the ER in

Author contributions: H.U., E.Y., T. Shimada, K.T., and I.H.-N. designed research; H.U. and N.K. performed research; H.U., E.Y., T. Shimmen, S.H., and V.V.D. contributed new reagents/analytic tools; H.U., N.K., and I.H.-N. analyzed data; and H.U., E.Y., V.V.D., and I.H.-N. wrote the paper.

The authors declare no conflict of interest.

*This Direct Submission article had a prearranged editor.

Freely available online through the PNAS open access option.

[1]To whom correspondence should be addressed. E-mail ihnishi@gr.bot.kyoto-u.ac.jp.

This article contains supporting information online at www.pnas.org/cgi/content/full/0911482107/DCSupplemental.

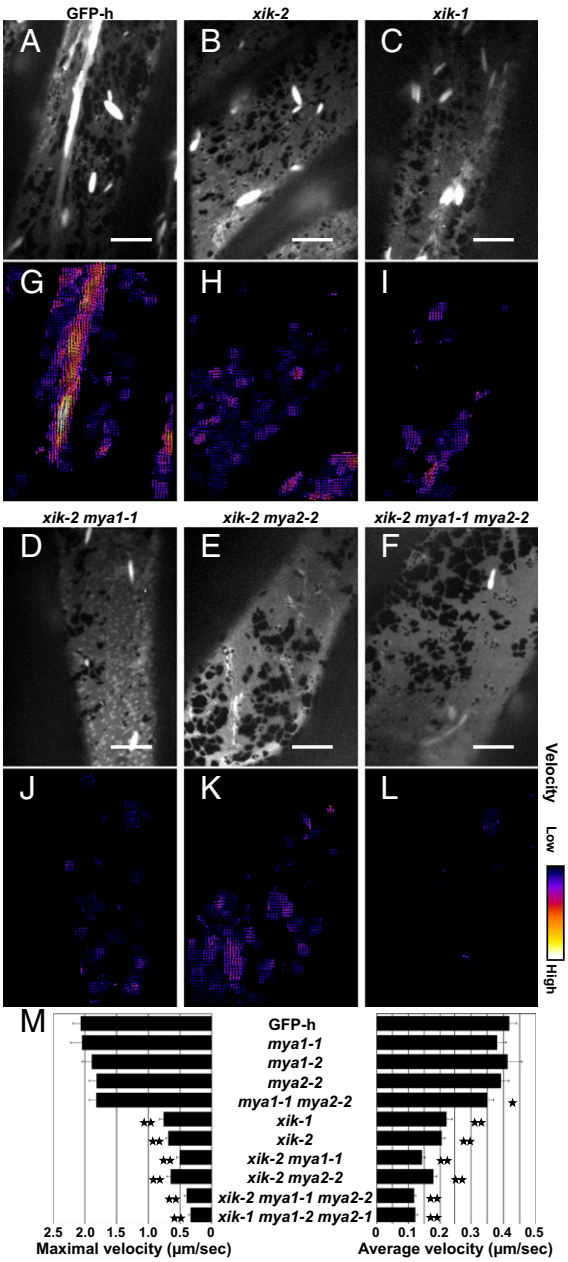

Fig. 1. ER streaming is suppressed in myosin XI-K–deficient mutants. Seven-day-old cotyledonary petioles of GFP-h and myosin XI mutants expressing ER-localized GFP were observed by spinning-disk confocal microscopy. One hundred time-lapse images of subperipheral ER were captured at ~50-ms intervals. Single mutants lacking myosin XI-K (*xik-1*, SALK_136682; *xik-2*, SALK_067972), MYA1/XI-1 (*mya1-1*, SALK_129098; *mya1-2*, SALK_022140), or MYA2/XI-2 (*mya2-1*, SALK_127984; *mya2-2*, SALK_055785) and double and triple mutants were generated. Maximum intensity projections (*A–F*) and velocity maps (*G–L*) of the GFP-h or mutant time-lapse images are shown. Bright spindle-shaped structures are ER bodies. (Scale bars, 10 μm.) Arrow lengths and colors in the maps indicate ER streaming velocities. (*M*) Maximal and average velocities (μm/sec) of ER streaming in GFP-h and mutants were calculated by KbiFlow software. Error bars represent SE. *, $P < 0.05$; **, $P < 0.001$ by Student's *t* test.

the peripheral plane was relatively static (Movie S1), whereas the ER in the inner plane was rapidly streaming (Movie S2).

To obtain an insight into the dynamics of cytosol per se, we used transgenic expression of a cytosolic form of GFP reporter. Interestingly, the streaming pattern of cytosolic GFP was similar to that of the ER-localized GFP (compare Movies S2 and S3, and Figs. S2 and S3). More specifically, the velocity map of cytosolic GFP also showed substantial degree of local variation (Fig. S3 *C* and *D*). By the KbiFlow analysis of 22 cells, maximal velocities for a peripheral and interior planes were 1.23 and 1.99 μm/sec ($P < 0.0005$ by Mann-Whitney test), and average velocities were 0.37 and 0.49 μm/sec ($P < 0.005$ by Mann-Whitney test), respectively (Table S1). These velocities were comparable to those of ER streaming in each focal plane (Table S1). Although the brightness of cytosolic GFP is a subject for multiple processes, such as local expression level, cytosol stirring, and mere thermal diffusion, so far cytosolic GFP provides the best approximation for a measure of cytoplasmic streaming. Therefore, these data suggest a correlation and a causative relationship between the streaming of ER and cytosol.

Myosin XI-K Is the Primary Contributor to ER Streaming. The ER dynamic was dose-dependently inhibited by the treatments with either latrunculin B (Lat B), an inhibitor of actin polymerization, or 2,3-butanedione monoxime (BDM), an inhibitor of myosin activity (Fig. S4 and Movies S4 and S5). Another inhibitor of actin polymerization, cytochalasin B, was also reported to inhibit the ER movement in onion epidermal cells (24). Taken together, these results suggested that the ER streaming requires both the active myosin motors and the intact actin cytoskeleton. To identify the myosins responsible for ER streaming, we analyzed gene knockout mutants in which three class XI myosins, XI-K, MYA1/XI-1, and MYA2/XI-2, that are ubiquitously expressed throughout the plants (http://atted.jp) (27, 28) were inactivated (Fig. S5).

Among the eight tested independent insertion mutant alleles (*mya1-1, mya1-2, mya2-1, mya2-2, xik-1, xik-2, xik-3*, and *xik-4*) (Fig. S5*A*), ER streaming was dramatically suppressed only in those targeting the myosin XI-K gene (Movie S6 for *xik-2*). The velocity maps of the ER streaming in *xik-1* and *xik-2* mutants showed obvious reductions in the number of bright arrows that represent high velocity streaming (Fig. 1 *H* and *I*) compared with that in the GFP-h map (Fig. 1*G*). The maximal and average ER velocities in each of the *xik-1* and *xik-2* mutants were only ~35 and ~50%, respectively, of those in GFP-h (Fig. 1*M* and Table S1).

We further obtained a series of five homozygous double- and triple-knockout mutants of the myosins XI-K, MYA1/XI-1, and MYA2/XI-2: *mya1 mya2* (*mya1-1 mya2-2*), *xik mya1* (*xik-2 mya1-1*), *xik mya2* (*xik-2 mya2-2*), and *xik mya1 mya2* (*xik-2 mya1-1 mya2-2* and *xik-1 mya1-2 mya2-1*). Among these mutants, the two triple mutants showed the strongest suppression of ER streaming (Fig. 1 and Movie S7). The average ER velocities in the triple mutants were ~30% of that in GFP-h, whereas the corresponding maximal velocities were reduced to less than ~20% (Fig. 1*M* and Table S1). On the other hand, ER streaming was slightly suppressed in the *mya1 mya2* double-gene knockout, but not in the *mya1* or *mya2* single-gene knockout mutants (Fig. 1*M* and Fig. S6). These results indicate that the myosin XI-K is the primary contributor to ER streaming, whereas the contributions of the myosins MYA1/XI-1 and MYA2/XI-2 are more limited.

In vitro motility assays have shown that the recombinant motor head of MYA1/XI-1, which is the most closely related myosin XI-K paralog, is able to translocate F-actin with a velocity of 3.2 μm/sec (29). The velocity of ER streaming measured here is up to 3.5 μm/sec (Fig. S2*E*), indicating that the myosin translocation velocities assayed in vitro and in vivo are similar.

Association of Myosin XI-K with ER. To determine if myosin XI-K is physically associated with ER, we generated a transgenic *Arabidopsis* line that constitutively expressed GFP fused with the C-terminal region of the myosin XI-K (GFP-XIKct), which harbored both a dimerization coiled-coil domain and a globular, cargo-binding, tail domain (30). Our attempts to use the GFP-XIKct reporter for direct microscopic observation of a potential association with ER were hampered by the strong fluorescence

CELL BIOLOGY

of the cytosolic pool of GFP-XIKct also observed by others (12, 17, 18). Because of that, we used subcellular fractionation as the means to separate ER from other cell components and to test for the presence of myosin XI-K in the ER-enriched fractions using antibodies specific to *Arabidopsis* myosin XI-K (14).

Sucrose-density gradient centrifugation of a microsomal fraction was performed in the presence of either $MgCl_2$ or EDTA to follow the shift in ER migration because of the release of ribosomes under EDTA treatment. It was found that the myosin XI-K peaked in the same gradient fractions as the ER marker BiP in the absence of Mg^{2+} (Fig. 2*A*). Furthermore, both myosin XI-K and BiP showed identical Mg^{2+}-dependent density shift in the gradients (Fig. 2*B*). These results demonstrated that a substantial fraction of the cellular pool of myosin XI-K comigrates with ER in the density gradients in a Mg^{2+}-dependent manner, and therefore is likely associated with ER.

On the other hand, there was no correspondence between the gradient peaks of the Golgi marker RGP1 and myosin XI-K (Fig. 2), an unexpected result given that the myosin XI-K inactivation suppresses the movements of Golgi bodies (14, 15). Because Golgi bodies are physically attached to the ER tubes (31), as is also obvious from the presence of Golgi marker in the peak ER fractions (Fig. 2), it seems possible that most of the myosin XI-K-containing Golgi bodies comigrate with the ER in gradients. Alternatively, because the overall surface of the ER is overwhelmingly larger than that of Golgi, the immunocytochemical signal from the ER-associated myosin is also much stronger than that from Golgi.

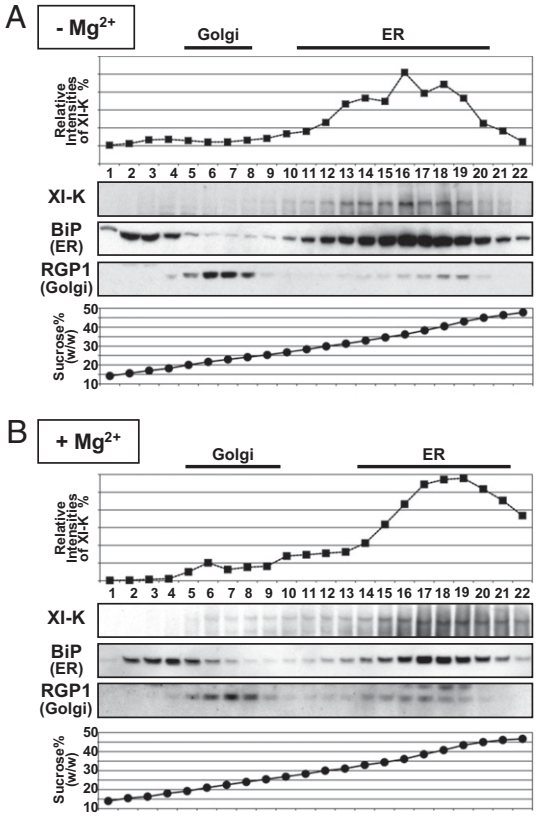

Fig. 2. Cofractionation of myosin XI-K with ER. Microsomal fractions prepared from 17-day-old plants in the presence of either EDTA ($-Mg^{2+}$) (*A*) or $MgCl_2$ ($+Mg^{2+}$) (*B*) were subjected to sucrose density gradient (15–50%, wt/wt) centrifugation in the presence of EDTA ($-Mg^{2+}$) (*A*) or $MgCl_2$ ($+Mg^{2+}$) (*B*). Fractions were subjected to immunoblot analysis with antibodies against myosin XI-K, BiP (ER marker), or RGP1 (Golgi marker).

Myosin XI-K Is Involved in Maintaining Spatial Configuration of the ER. As seen in Fig. 1, inactivation of the myosin XI-K affected not only the ER movement but also the formation of thick, highly mobile ER strands, suggesting that myosin XI-K is required for the proper spatial configuration of the ER. More detailed analysis of the ER network revealed defects in the development of the transvacuolar cytoplasmic strands formed by the AF bundles in the *xik* knockout mutants (Fig. 3 *A–C*). This result is consistent with the previous reports of the reduced number of transvacuolar strands upon BDM treatment (32, 33). Additionally, multiple myosin knockout mutants had unevenly distributed thick, sheet-like structures of the ER network (Fig. 3*E*) and large ER aggregates mainly at the cell edges (Fig. 3 *F* and *G* and Movie S8, discussed below). These abnormal ER configurations were most evident in the *xik mya1 mya2* triple knockout, whereas double-knockout *mya1 mya2* had no obvious abnormality (Fig. S6*D*).

In addition to regular ER network, *Arabidopsis* cells possess ER-derived spindle-shaped organelles, called ER bodies, which are observed to stream in the cortical region and transvacuolar strands of the epidermal cells of the seedlings (Fig. S7 *A–C*). The ER bodies in *xik mya1 mya2* triple knockout exhibited abnormally elongated shapes and distribution, often accumulating as concatemers in a perinuclear region (Fig. 3*G*, and Fig. S7 *D–F*). Double-knockout mutants *xik mya2* and *xik mya1* showed a milder phenotype than the triple mutant. Taken together, these results suggest that the ER-associated myosin XI-K is involved in maintaining the proper ER organization and determining the size and distribution of the ER bodies by driving the ER streaming.

Reorganization of the AF Bundles in Myosin XI-K-Deficient Mutants. In accord with the known role of the actin cytoskeleton in ER network organization (34), we have observed the abnormal ER configuration in the wild-type cells treated with Lat B to disassemble AFs (Fig. S4 *B–D*). To further examine the relationships between the ER network and the actin cytoskeleton in the myosin-deficient plants, we generated transgenic lines that expressed both the ER-localized GFP and the F-actin marker tdTomato-ABD2 based on the improved variant of the red-fluorescent protein (35, 36).

The epidermal cells of cotyledonary petioles in the Columbia-0 (Col-0) background exhibited thick, longitudinally oriented AF bundles, with the ER streaming occurring along these bundles (Fig. 4*A*). Strikingly, the AF bundles were randomly oriented in a double-myosin knockout *xik mya2*, whereas the typical ER strands were mostly absent (Fig. 4*B*). The double mutant also exhibited abnormal distributions of the ER (the thick, sheet-like structures and large aggregates of the ER), as did the triple-mutant *xik mya1 mya2* (Fig. 3 *E–G*). Collectively, these results suggest that the ER strand formation involves myosin XI-dependent, dynamic bridging of the ER subdomains, such as tubules and amorphous cisternae, to the AF. Rapid, directional transport of these subdomains results in their orientation and concentration along the AF bundles, producing motile, brightly fluorescent ER strands.

We quantitatively analyzed the orientation of the AF-bundles labeled with tdTomato-ABD2 by image processing (Fig. S8*A*). Statistical analysis of 24 to ~26 cells showed that the average angle of the AFs against longitudinal axis of the cell in *xik mya2* was larger than that in Col-0 ($P < 0.05$ by Student's *t* test), whereas the parallelness of AFs in *xik mya2* was lower than that in Col-0 ($P < 0.001$ by Student's *t* test) (Fig. 4*C*). To exclude the possibility that the organization of AF bundles was affected by the overexpression of tdTomato-ABD2 reporter, endogenous AFs in the nontransgenic plants were observed by Alexa 546–phalloidin staining (Fig. S9). In the double and triple knockouts *xik mya2* and *xik-2 mya1-1 mya2-2*, the AF bundles again showed random distribution with some bundles oriented perpendicularly to the longitudinal direction of the cell (Fig. S9 *G*, *H*, *J*, and *K*). In contrast, this pattern was rarely observed in the Col-0, *mya1*, *mya2*, *mya1 mya2*, *xik*, and *xik mya1* backgrounds (Fig. S9 *A–F*

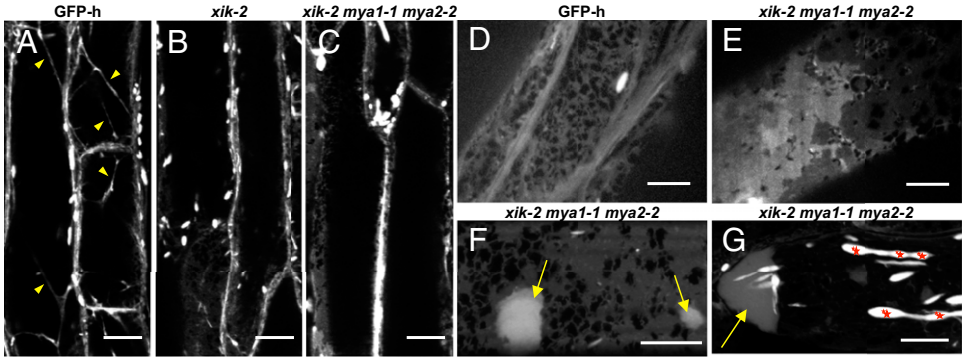

Fig. 3. Myosin XI-K deficiency induces an aberrant ER configuration. Maximum-intensity projections of 8-day-old (*A–C*) or 7-day-old (*D–G*) GFP-h (*A, D*), *xik-2* (*B*), and *xik-2 mya1-1 mya2-2* (*C, E–G*) cotyledonary petioles expressing ER-localized GFP observed by laser-scanning confocal microscopy (*A–C, F, G*) or spinning-disk confocal microscopy (*D, E*). Projections were reconstituted from six (*A–C*) or four (*F, G*) sequential images taken along the optical *z* axis (1-μm intervals) or from 100 time-sequential images of subperipheral ER captured at ∼50-ms intervals (*D, E*). Bright spindle-shaped structures are ER bodies. Arrowheads in *A* indicate transvacuolar strands; yellow arrows in *F* and *G* indicate ER aggregates; red asterisks in *G* indicate abnormally shaped ER bodies. (Scale bars, 20 μm in *A–C* or 10 μm in *D–G*.)

and *I*). Myosin XI-K deficiency had a significant effect on ER motility (Fig. 1), but did not noticeably alter actin organization.

Similar phenomena were revealed in the epidermal cells of the etiolated hypocotyls. Col-0 hypocotyls had thick, longitudinally oriented AF bundles, with the ER streaming occurring along these bundles (Fig. S8 *B* and *D* and Movie S9), and *xik mya2* hypocotyls, which had randomly oriented AF bundles, exhibited neither ER strands nor streaming (Fig. S8 *C* and *D*, Movie S10).

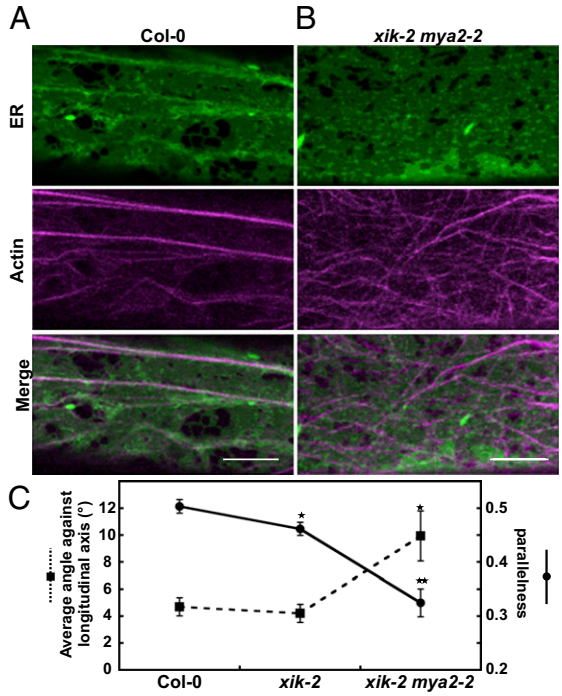

Fig. 4. Myosin XI-K deficiency induces AF-bundle disorganization. Seven-day-old cotyledonary petioles of Col-0 (*A*) and *xik-2 mya2-2* (*B*) expressing ER-localized GFP and tdTomato-ABD2 were observed by laser-scanning confocal microscopy. Maximum intensity projections were reconstituted from three sequential images taken along the optical *z* axis (0.5-μm intervals). (Scale bars, 10 μm.) (*C*) Orientation of AF-bundles was evaluated by two indices: Average angle of AF-bundles against a longitudinal axis and parallelness. Error bars represent SE. *, $P < 0.05$; **, $P < 0.001$ by Student's *t* test ($n = 24–26$).

These results indicated that the myosins XI-K and MYA2/XI-2 are collectively required for the maintenance of the thick AF bundles and associated ER strands, at least in the certain types of the elongated cells. As recently proposed by Staiger et al. (37), plant myosins could play a role in the constant buckling and straightening of AFs. Our data provide experimental evidence supporting the emerging concept of the myosin-dependent AF dynamics required for the formation and positioning of the AF bundles.

Conclusions. Our findings provide unique insight into the mechanisms of the actomyosin-driven intracellular motility in higher plants. We find that the myosin XI-K is associated with ER and acts as the primary contributor to the ER streaming. We further show that the myosin XI-K in cooperation with the myosin MYA2/XI-2 is involved in organizing AF bundles and the associated ER strands. To address the significance and the outcome of the three-way interactions among ER, AFs, and myosins, we propose a model involving a positive-feedback loop. Initially, the myosin-associated ER subdomains slide along randomly oriented actin filaments (or immature AF bundles). Such ER sliding gradually promotes formation of the unidirectionally oriented, thick AF bundles by aligning the adjacent AF bundles through the ER-associated myosins. Reiteration of this process in the elongated cells results in a formation of a few, longitudinally oriented, thick AF bundles that provide tracks for the extensive streaming of the ER strands. Because the ER network is the largest cellular endomembrane system, it seems to be a natural candidate for the anchoring and aligning multiple AFs throughout the elongated cells. Furthermore, the large mass and surface area of the unidirectionally streaming ER is likely to haul the cytosol along, resulting in a concomitant passive cytoplasmic streaming. Our results, showing similar patterns and velocities of the ER and cytosol streaming, are well compatible with this concept.

Materials and Methods

Plant Materials and Growth Conditions. *Arabidopsis thaliana* ecotype Col-0 was used as the wild-type plant. We used the following *Arabidopsis* transgenic lines: GFP-h (38), and the plants expressing cytosolic GFP (39). Seeds of *Arabidopsis* were surface-sterilized and then sown onto 0.5% Gellan Gum (Wako), which contained 1% sucrose and Murasige-Skoog's medium. After incubation for 3 to 5 days at 4 °C to break seed dormancy, the plants were grown at 22 °C under continuous light.

Imaging of ER Streaming. We used abaxial epidermal cells in 7-day-old cotyledonary petioles for the imaging of ER streaming.

We analyzed two ∼1-μm thick optical planes at ∼1.5 μm distance, a peripheral plane and an interior plane, for Figs. S2 and S3 and a subperipheral

CELL BIOLOGY

focal plane located between these planes for Fig. 1 and Figs. S4 and S6. The ER streaming was observed with a fluorescence microscope (Axioplan 2 Imaging, Carl Zeiss) equipped with a confocal laser scanning unit (CSU 10, Yokogawa Electric) and the laser unit (Sapphire 488 Coherent). We collected the time-lapse images of ER by an EM-CCD camera (C9100, Hamamatsu Photonics) with a 100 × 1.45 numerical aperture oil-immersion objective. For each cell, 100 frames were continuously scanned during ~5.4 s (frame rate: 50 ms per frame). ER streaming was analyzed using our in-house developed plug-in package, KbiFlow, for ImageJ software (National Institutes of Health; *SI Materials and Methods*). The KBI plug-in package can be downloaded for free from http://hasezawa.ib.k.u-tokyo.ac.jp/zp/Kbi/ImageJKbiPlugins.

Myosin XI-Deficient Mutants. T-DNA-tagged mutants of XI-K, MYA1/XI-1, and MYA2/XI-2 were established (Fig. S5). Double and triple mutants of myosin XI were generated by crossing single mutants. Seeds of T-DNA-tagged mutants were obtained from the Salk Institute Genomic Analysis Laboratory. *mya2-1* was described previously (10). To visualize ER in myosin XI-deficient mutants, single mutants were crossed with GFP-h. Alternatively, a *SP-GFP-HDEL* gene (40) was stably transformed into double and triple mutants via *Agrobacterium*.

Plasmid Construction and Transformation. DNA sequence corresponding to C-terminal tail region of XI-K (XIKct) was amplified by PCR with a cDNA library prepared from *Arabidopsis* Col-0 and KOD plus polymerase (Toyobo). A pair of specific primers (XI-K-CT-for, 5′-caccCTTAAGATGGCCGCACGAGACACA-3′; and XI-K-CT-rev, 5′-TTACGATGTACTGCCTTCTTTACGTGT-3′) was used. Amplified fragments were subcloned into pENTR/D-TOPO using Gateway TOPO cloning kit (Invitrogen) and sequenced. To express XIKct as a GFP-XIKct fusion protein, the *XIK* construct was introduced into pGWB406 plant expression vector by LR reaction of the Gateway system (Invitrogen) (41). The construct was introduced into *Arabidopsis* Col-0 plants by the floral-dip method (42).

Subcellular Fractionation. The aerial parts of 17-day-old GFP-XIKct plants (1.5 g fresh weight) were chopped with a razor blade in a Petri dish on ice in 6 mL of 5 mM EDTA or 5 mM $MgCl_2$ and 5 mM EGTA in extraction buffer (30 mM Pipes-KOH, pH 7.0, 0.4 M sucrose, 1 mM DTT, 1 mM PMSF, 0.1 mg/mL leupeptin and 1% casein). The homogenate was filtered through a Cell Strainer (70 μm) by centrifugation at 50 × *g*. An aliquot of the filtrate was used as the total fraction. The microsomal fractions were prepared by sequential centrifugations of the total fraction at 2,000 × *g* for 20 min and 100,000 × *g* for 1 h. The 100,000 × *g* pellets were resuspended in 0.2 mL of the extraction buffer without 1% casein in the presence of 5 mM EDTA or 5 mM $MgCl_2$ and 5 mM EGTA and layered directly on top of a 16-mL linear sucrose density gradient (15–50%, wt/wt). Centrifugation was performed in an SW28.1 rotor (Beckman) at 25,000 rpm for 20 h at 4 °C, and 700-μL fractions were collected with a piston gradient fractionator (TOWA LABO). Each fraction was concentrated with acetone and subjected to SDS/PAGE and immunoblot analyses, as described previously (43). Antibodies used were anti-XI-K (diluted 5,000-fold) (14), anti-BiP (diluted 10,000-fold) (44), and anti-RGP1 (diluted 10,000-fold) (45).

Confocal Laser Scanning Microscopy. The fluorescent images were inspected with a confocal laser scanning microscope (LSM510 META; Carl Zeiss) using the 488-nm line of a 40-mW Ar/Kr laser or the 543-nm line of a 1-mW He/Ne laser with either a 63 × 1.2 numerical aperture water-immersion objective or a 20 × 0.8 numerical aperture dry objective. The data were processed using Adobe Photoshop (Adobe Systems) or ImageJ.

Visualization of AFs. AFs were visualized with tdTomato-ABD2 which expresses actin binding domain 2 of *Arabidopsis thaliana* Fimbrin 1 (ABD2 AtFim1) fused to tdTomato (35, 36). We stably introduced this construct into GFP-h or myosin XI mutants that expressed ER-localized GFP. Because homozygous *tdTomato-ABD2* caused delay of growth to *xik mya2*, we used the *xik mya2* plants with heterozygous *tdTomato-ABD2* in which the growth rates were similar to those in *xik mya2*. Orientation of AF-bundles was analyzed using our in-house developed plug-in package, KbiLineExtract, for ImageJ software (Fig. S8*A*) (*SI Materials and Methods*).

ACKNOWLEDGMENTS. We thank Drs. S. Mano and M. Nishimura (National Institute for Basic Biology) for donating transgenic *Arabidopsis* expressing cytosolic GFP, Drs. P. M. Ray and K. S. Dhugga (Stanford University) for providing anti-pea RGP1 antibody, Dr. T. Higaki (The University of Tokyo) for providing the *Arabidopsis ABD2 Fim1* gene in the pUC18 vector, and Dr. T. Nakagawa (Shimane University) for providing pGWB406. This work was supported by Grants-in-Aid for Scientific Research from the Ministry of Education, Culture, Sports, Science and Technology (MEXT) of Japan Grants 16085203 and 17107002 (to I.H.-N.) and Grants 20770032 and 21200065 (to H. U.), and by the Global Center of Excellence Program "Formation of a Strategic Base for Biodiversity and Evolutionary Research: from Genome to Ecosystem" of MEXT. The work in the V.V.D. laboratory is supported by a National Institutes of Health American Recovery and Reinvestment Act award (GM087658).

1. Corti B (1774) *Osservazioni microscopiche sulla Tremella: e sulla circolazione del fluido in una pianta acquajuola* (Apresso Giuseppe Rocchi, Lucca).
2. Grolig F, Pierson ES (2000) *Actin: A Dynamic Framework for Multiple Plant Cell Functions*, eds Staiger CJ, Baluska F, Volkmann D, Barlow P (Kluwer Academic Publishers, Dordrecht, The Netherlands), pp 165–190.
3. Shimmen T, Yokota E (2004) Cytoplasmic streaming in plants. *Curr Opin Cell Biol* 16: 68–72.
4. Shimmen T (2007) The sliding theory of cytoplasmic streaming: fifty years of progress. *J Plant Res* 120:31–43.
5. Yokota E, Yukawa C, Muto S, Sonobe S, Shimmen T (1999) Biochemical and immunocytochemical characterization of two types of myosins in cultured tobacco bright yellow-2 cells. *Plant Physiol* 121:525–534.
6. Tominaga M, et al. (2003) Higher plant myosin XI moves processively on actin with 35 nm steps at high velocity. *EMBO J* 22:1263–1272.
7. Yokota E, et al. (1995) Localization of a 170 kDa myosin heavy chain in plant cells. *Protoplasma* 185:178–187.
8. Liu L, Zhou J, Pesacreta TC (2001) Maize myosins: diversity, localization, and function. *Cell Motil Cytoskeleton* 48:130–148.
9. Wang Z, Pesacreta TC (2004) A subclass of myosin XI is associated with mitochondria, plastids, and the molecular chaperone subunit TCP-1alpha in maize. *Cell Motil Cytoskeleton* 57:218–232.
10. Hashimoto K, et al. (2005) Peroxisomal localization of a myosin XI isoform in *Arabidopsis thaliana*. *Plant Cell Physiol* 46:782–789.
11. Romagnoli S, et al. (2007) Microtubule- and actin filament-dependent motors are distributed on pollen tube mitochondria and contribute differently to their movement. *Plant Cell Physiol* 48:345–361.
12. Reisen D, Hanson MR (2007) Association of six YFP-myosin XI-tail fusions with mobile plant cell organelles. *BMC Plant Biol* 7:6.
13. Li JF, Nebenführ A (2007) Organelle targeting of myosin XI is mediated by two globular tail subdomains with separate cargo binding sites. *J Biol Chem* 282:20593–20602.
14. Peremyslov VV, Prokhnevsky AI, Avisar D, Dolja VV (2008) Two class XI myosins function in organelle trafficking and root hair development in *Arabidopsis*. *Plant Physiol* 146:1109–1116.
15. Prokhnevsky AI, Peremyslov VV, Dolja VV (2008) Overlapping functions of the four class XI myosins in *Arabidopsis* growth, root hair elongation, and organelle motility. *Proc Natl Acad Sci USA* 105:19744–19749.
16. Avisar D, Prokhnevsky AI, Makarova KS, Koonin EV, Dolja VV (2008) Myosin XI-K Is required for rapid trafficking of Golgi stacks, peroxisomes, and mitochondria in leaf cells of *Nicotiana benthamiana*. *Plant Physiol* 146:1098–1108.
17. Sparkes IA, Teanby NA, Hawes C (2008) Truncated myosin XI tail fusions inhibit peroxisome, Golgi, and mitochondrial movement in tobacco leaf epidermal cells: a genetic tool for the next generation. *J Exp Bot* 59:2499–2512.
18. Avisar D, et al. (2009) A comparative study of the involvement of 17 *Arabidopsis* myosin family members on the motility of Golgi and other organelles. *Plant Physiol* 150:700–709.
19. Lichtscheidl IK, Baluska F. (2000) *in Actin: A Dynamic Framework for Multiple Plant Cell Functions*, eds Staiger CJ, Baluska F, Volkmann D, Barlow P (Kluwer Academic Publishers,Dordrecht, The Netherlands), Vol. Developments in Plant and Soil Sciences, Vol. 89, pp 191–201.
20. Voeltz GK, Rolls MM, Rapoport TA (2002) Structural organization of the endoplasmic reticulum. *EMBO Rep* 3:944–950.
21. Quader H, Zachariadis M (2006) *in The Plant Endoplasmic Reticulum*, ed Robinson DG (Springer,Berlin / Heidelberg), Vol. Plant Cell Monographs, pp 1–23.
22. Borgese N, Francolini M, Snapp E (2006) Endoplasmic reticulum architecture: structures in flux. *Curr Opin Cell Biol* 18:358–364.
23. Quader H, Schnepf E (1986) Endoplasmic reticulum and cytoplasmic streaming: Fluorescence microscopical observations in adaxial epidermis cells of onion bulb scales. *Protoplasma* 131:250–252.
24. Allen NS, Brown DT (1988) Dynamics of the endoplasmic reticulum in living onion epidermal cells in relation to microtubules, microfilaments, and intracellular particle movement. *Cell Motil Cytoskeleton* 10:153–163.
25. Boevink P, et al. (1996) Virus-mediated delivery of the green fluorescent protein to the endoplasmic reticulum of plant cells. *Plant J* 10:935–941.
26. Yokota E, et al. (2009) An isoform of myosin XI is responsible for the translocation of endoplasmic reticulum in tobacco cultured BY-2 cells. *J Exp Bot* 60:197–212.
27. Obayashi T, Hayashi S, Saeki M, Ohta H, Kinoshita K (2009) ATTED-II provides coexpressed gene networks for *Arabidopsis*. *Nucleic Acids Res* 37 (Database issue): D987–D991.
28. Ojangu EL, Järve K, Paves H, Truve E (2007) *Arabidopsis thaliana* myosin XIK is involved in root hair as well as trichome morphogenesis on stems and leaves. *Protoplasma* 230: 193–202.

29. Hachikubo Y, Ito K, Schiefelbein J, Manstein DJ, Yamamoto K (2007) Enzymatic activity and motility of recombinant *Arabidopsis* myosin XI, MYA1. *Plant Cell Physiol* 48:886–891.
30. Reddy AS, Day IS (2001) Analysis of the myosins encoded in the recently completed *Arabidopsis thaliana* genome sequence. *Genome Biol* 2: RESEARCH0024.1-0024.17.
31. Sparkes IA, Ketelaar T, Ruijter NC, Hawes C (2009) Grab a Golgi: Laser trapping of Golgi bodies reveals in vivo interactions with the endoplasmic reticulum. *Traffic* 10: 567–571.
32. Hoffmann A, Nebenführ A (2004) Dynamic rearrangements of transvacuolar strands in BY-2 cells imply a role of myosin in remodeling the plant actin cytoskeleton. *Protoplasma* 224:201–210.
33. Holweg CL (2007) Living markers for actin block myosin-dependent motility of plant organelles and auxin. *Cell Motil Cytoskeleton* 64:69–81.
34. Boevink P, et al. (1998) Stacks on tracks: the plant Golgi apparatus traffics on an actin/ER network. *Plant J* 15:441–447.
35. Higaki T, Kutsuna N, Okubo E, Sano T, Hasezawa S (2006) Actin microfilaments regulate vacuolar structures and dynamics: dual observation of actin microfilaments and vacuolar membrane in living tobacco BY-2 Cells. *Plant Cell Physiol* 47:839–852.
36. Nakano RT, et al. (2009) GNOM-LIKE1/ERMO1 and SEC24a/ERMO2 are required for maintenance of endoplasmic reticulum morphology in *Arabidopsis thaliana*. *Plant Cell* 21:3672–3685.
37. Staiger CJ, et al. (2009) Actin filament dynamics are dominated by rapid growth and severing activity in the *Arabidopsis* cortical array. *J Cell Biol* 184:269–280.
38. Matsushima R, et al. (2003) The ER body, a novel endoplasmic reticulum-derived structure in *Arabidopsis*. *Plant Cell Physiol* 44:661–666.
39. Mano S, et al. (2002) Distribution and characterization of peroxisomes in *Arabidopsis* by visualization with GFP: dynamic morphology and actin-dependent movement. *Plant Cell Physiol* 43:331–341.
40. Mitsuhashi N, Shimada T, Mano S, Nishimura M, Hara-Nishimura I (2000) Characterization of organelles in the vacuolar-sorting pathway by visualization with GFP in tobacco BY-2 cells. *Plant Cell Physiol* 41:993–1001.
41. Nakagawa T, et al. (2007) Improved Gateway binary vectors: high-performance vectors for creation of fusion constructs in transgenic analysis of plants. *Biosci Biotechnol Biochem* 71:2095–2100.
42. Clough SJ, Bent AF (1998) Floral dip: a simplified method for Agrobacterium-mediated transformation of *Arabidopsis thaliana*. *Plant J* 16:735–743.
43. Shimada T, et al. (2003) Vacuolar processing enzymes are essential for proper processing of seed storage proteins in *Arabidopsis thaliana*. *J Biol Chem* 278: 32292–32299.
44. Hatano K, Shimada T, Hiraiwa N, Nishimura M, Hara-Nishimura I (1997) A rapid increase in the level of binding protein (BiP) is accompanied by synthesis and degradation of storage proteins in pumpkin cotyledons. *Plant Cell Physiol* 38:344–351.
45. Dhugga KS, Tiwari SC, Ray PM (1997) A reversibly glycosylated polypeptide (RGP1) possibly involved in plant cell wall synthesis: purification, gene cloning, and trans-Golgi localization. *Proc Natl Acad Sci USA* 94:7679–7684.